Extension of excitation functions of proton-induced reactions on bismuth

L. Mokhtari Oranj,[1] M. Bakhtiari,[2] N. S. Jung,[1] A. Lee,[1] and H. S. Lee[1,2,*]
[1]*Pohang Accelerator Laboratory, POSTECH, Pohang 37673, Republic of Korea*
[2]*Division of Advanced Nuclear Engineering, POSTECH, Pohang 37673, Republic of Korea*

(Received 28 July 2019; revised manuscript received 3 November 2019; published 6 January 2020)

Production cross sections for ^{209}Bi(p, xn)^{207,206,205,204}Po and ^{209}Bi(p, pxn)^{207,206,205,204,203}Bi reactions were measured using the stacked-foil technique. In our previous work, excitation functions of the mentioned reactions were measured at proton energies from 60 to 100 MeV. In this work, the excitation functions of the reactions are extended down to the proton energy of 40 MeV. Two targets were arranged in two different stacks including Bi, Al, and Au foils as well as Bi and Pb plates. After the irradiations, production yields of interested radionuclei were measured by γ-ray spectroscopy system using HPGe detectors. Proton beam intensities were measured using ^{27}Al(p, $3pn$)^{24}Na, ^{197}Au(p, $p3n$)^{194}Au, and ^{197}Au(p, pn)^{196}Au monitor reactions. More than 50 cross-section data points were measured, including independent and cumulative cross sections. A similar trend was found between the data measured in this work and our earlier work. Our measured data were consistent with the experimental data in the literature. Excitation functions of the investigated reactions were also calculated using the TALYS-1.9 code with six different level density models. The results showed that phenomenological level density models predicted higher cross-section value than the microscopic level density models for the ^{209}Bi(p, xn) reactions. However, microscopic level density models indicated higher calculated cross sections for the ^{209}Bi(p, pxn) reactions.

DOI: 10.1103/PhysRevC.101.014602

I. INTRODUCTION

Production cross section of radionuclei generated by proton-induced reactions are vital in different fields of applied physics as accelerator design, space technology, and radionuclide production in radiopharmacy [1]. Bismuth is one material which is gaining interest in nuclear technologies as in the radiation shielding and is also a suitable target in the accelerator-driven systems [2,3]. Therefore, nuclear data for proton-induced reactions on bismuth play a leading role in such areas. Several studies on Bi bombarded with protons have been reported [3–12]. However, there is still a lack of the experimental cross-section data in the tens-MeV energies.

In our previous work, the production cross sections of the reactions, ^{209}Bi(p, xn)^{207,206,205,204,203}Po, ^{209}Bi(p, pxn)^{207,206,205,204,203,202}Bi, and ^{nat}Pb(p, xn)^{206,205,204,203,202,201}Bi in the energy range of 60 to 100 MeV were measured [13]. In this study, the cross sections of ^{209}Bi(p, xn)^{207,206,205,204}Po and ^{209}Bi(p, pxn)^{207,206,205,204,203}Bi were measured in the energy range of 40 to 69 MeV by performing two experiment rounds to extend the cross-section data of these reactions to lower energy ranges. At this energy range, compound and precompound mechanisms become much more dominant and the peak of the excitation functions of the ^{209}Bi(p, xn) reactions are located at below 70 MeV. Because of significant variation of cross sections with small change in proton energy, it is crucial to conduct more experiments. Furthermore, excitation functions of the mentioned reactions were calculated using TALYS-1.9 [14] using different nuclear level densities (NLD) models.

The goal of this work is to increase the nuclear data libraries for proton-induced reactions on heavy materials for practical applications since the experimental data in this energy range are rare and also to asses the capability of the nuclear model calculations.

II. METHODS

A. Target preparation

Two experiment rounds were carried out at Korea Multipurpose Accelerator Complex (KOMAC). The experiments were performed using the well-known stacked-foil technique. Two targets were prepared for the experiments so that Bi activation and Al and Au monitoring foils were sandwiched between two Al foils to avoid cross contamination and recoil effects. In the first experiment, an Al foil (100 μm, 2.69 gcm^{-3}, 99.99%) was used to monitor the beam intensity. Natural bismuth plates were placed in the stack as the energy degrader. In the second round, one Au (30 μm, 19.3 g cm^{-3}, 99.99%) and one Al foil (100 μm, 2.69 g cm^{-3}, 99.99%) were used as the monitoring foils. Natural lead plates were the energy degraders. In each experiment, five bismuth foils (50 μm, 9.8 g cm^{-3}, 99.97%) were used as the activation foils. The cross-sectional size of all foils was 5 × 5 cm. Total thickness of targets were 1.05 and 0.91 cm for the first and second experiments, respectively. The total thickness of each stack was larger than the range of 69-MeV protons, calculated by SRIM-2010 [15].

*Corresponding author: lee@postech.ac.kr

B. γ-ray spectrum and data analysis

γ-ray spectrum analysis of activation foils started after a cooling time of 30 min for both experiments. HPGe detectors with relative efficiencies of 15% and 20% were used for γ-ray spectra measurement. The energy resolution of detectors were 1.71-keV full-width at half-maximum (FWHM) at the 1.33-MeV peak of ^{60}Co. The dead time was less than 4.5% during the measurement by placing the activated samples at proper distances. The absolute efficiency of HPGe detectors were obtained using standard multiple γ-ray sources within 10 cm of source-to-detector distance. Regarding the half-life of a radionuclide, the γ-ray spectrum analysis was performed several times. Canberra's Genie-2000 (version 3.2) [16] γ-ray analysis software was used for analyzing γ-ray spectra.

C. Determination of proton energy and intensity

The two stacked foils were irradiated for 240 and 25 s by 69-MeV protons, respectively, with the repetition rate of 1 Hz. The beam shape was described by Gaussian distribution at the target in both x and y directions (z is the beam direction) based on the beam profile on the Gafchromic film.

The energy distribution of protons onto the Bi activation foils was obtained using FLUKA Monte Carlo code [17]. According to FLUKA calculations, the incident energies of protons impinging each Bi foil were 68.1 ± 0.3, 62.8 ± 0.8, 57.0 ± 1.1, 50.8 ± 1.5, and 44.1 ± 1.6 MeV for the first experiment and 67.4 ± 0.3, 61.3 ± 0.8, 54.7 ± 1.1, 47.5 ± 1.4, and 43.1 ± 1.6 MeV for the second experiment. In our previous work [13], it was proved that the contribution of secondary neutrons and protons to the measured cross sections were negligible as the proton energy was 100 MeV, which is quite higher than the proton energy in this work.

In the first experiment, proton beam intensity was measured by activation analysis method using the monitor reaction ^{27}Al(p, $3pn$)^{24}Na, and for the second experiment, ^{27}Al(p, $3pn$)^{24}Na, ^{197}Au(p, pn)^{196}Au, and ^{197}Au(p, $p3n$)^{194}Au reactions were used. To obtain the beam intensity, cross sections of the monitor reactions were taken from Refs. [18,19]. The decay data of all radionuclei were taken from Ref. [20] and are listed in Tables I and II. Measured production yields of monitor reactions for both experiments and relevant proton beam intensities are given in Table III. Uncertainty of the beam intensities for each experiment was obtained by including all possible uncertainties of measured activities (2%), applied cross section (10%), and mass of the monitor foils (≈0.01%). The final uncertainty of the measured beam intensities in the first and second experiments was approximately 10.2%. To obtain the cross-section values in the second experiment, an average beam intensity was adopted.

D. Nuclear model calculations

In order to understand the capability of nuclear models in estimation of nuclear reaction cross sections, theoretical calculations were performed by means of the TALYS-1.9 [14] code. TALYS is a nuclear model calculation code in which photons, neutrons, protons, ^{3}He, and ^{4}He can be used as projectiles in the energy range of 1 keV to 200 MeV for target elements with mass of 12 and heavier [14].

As default, the TALYS code uses the constant temperature model (CTM) [21] at low energies, and the Fermi gas model (FGM) [22] at higher energies for NLDs, global optical model potential (OMP) of Koning and Delaroche [23] for OMPs, and it uses γ-ray transmission coefficients, which are generated with the Kopecky-Uhl generalized Lorentzian, for the γ-ray strength functions (γSFs) [24]. Pre-equilibrium reactions that become far more dominant at energies higher than around 10 MeV are modeled according to two-exciton model [14]. It is known that nuclear cross sections are dependent on NLDs, OMPs, and γSFs [25–27]. In the Hauser-Feshbach model [28], (a) spin parity of the target and residual nuclei, (b) transmission coefficients of outgoing particles, and (c) photon transmission coefficients are the main ingredients. In the TALYS code, spins and parities could be read from a table or calculated using a NLD model, transmission coefficients of particles are calculated by means of OMP, and photon transmission coefficients are obtained from γSF models. In Refs. [29,30], we considered the effects of TALYS nuclear models on reaction cross sections. Moreover, in our previous work [13], it was concluded that NLDs were the most effective nuclear models to the reaction cross sections rather than OMPs and γSFs. Therefore, the influence of only NLDs are considered in this work.

There are six different NLD models that can be implemented in the TALYS code to consider their influence on the nuclear reaction cross section. Phenomenological and microscopic NLD models that have been applied in the TALYS calculations are listed in Table IV. In the results section, the theoretical calculations are compared to the measured data.

TABLE I. Decay characteristic of monitor reactions [20].

Nuclide	Half-life	E_γ (keV)	I_γ (%)	Contributing reactions	Q value (MeV)
^{196}Au	6.1669 ± 0.0006 d	333.03	22.9 ± 0.9	^{197}Au(p, pn)	− 8.07
		355.73	87 ± 3		
^{194}Au	38.02 ± 0.1 h	293.548	10.6 ± 0.15	^{197}Au(p, $p3n$)	−23.29
		328.464	60.4 ± 0.8		
^{24}Na	14.997 ± 0.012 h	1368.626	99.9936 ± 0.0015	^{27}Al(p, $3pn$)	−31.43
		2754.007	99.855 ± 0.005		

TABLE II. Decay characteristic of measured radionuclei [20].

Nuclide	Half-life	E_γ (keV)	I_γ (%)	Contributing reactions	Q value (MeV)
^{207}Po	5.80 ± 0.02 h	405.78	9.7 ± 0.1	^{209}Bi(p, 3n) ^{207}Po →^{207}Bi	−18.04
		742.72	28.4 ± 0.7		
		911.77	17.0 ± 0.4		
		992.39	59.2 ± 1.3		
^{206}Po	8.8 ± 0.1 d	286.41	22.9 ± 0.5	^{209}Bi(p, 4n) ^{206}Po →^{206}Bi	−25.07
		338.44	18.5 ± 0.4		
		522.47	15.1 ± 0.4		
		807.38	21.8 ± 0.5		
		980.23	6.81 ± 0.16		
		1032.26	31.7 ± 0.8		
^{205}Po	1.74 ± 0.08 h	836.8	19.2 ± 1.5	^{209}Bi(p, 5n) ^{205}Po →^{205}Bi	−33.82
		849.8	25.5 ± 2		
		872.4	37 ± 2		
		1001.2	28.8 ± 2.1		
^{204}Po	3.519 ± 0.012 h	270.06	31.9 ± 1.1	^{209}Bi(p, 6n) ^{204}Po →^{204}Bi	−41.05
		762.52	13.2 ± 0.4		
		883.96	34.3 ± 0.8		
		1016.29	27.6 ± 0.7		
^{207}Bi	31.55 ± 0.04 yr	569.698	97.75 ± 0.03	^{209}Bi(p, $p2n$)^{207}Bi	−14.35
		1063.656	74.5 ± 0.3		
^{206}Bi	6.243 ± 0.003 d	183.977	15.8 ± 0.3	^{209}Bi(p, $p3n$)^{206}Bi	−22.44
		343.51	23.5 ± 0.4		
		398.00	10.75 ± 0.15		
		497.06	15.33 ± 0.21		
		516.18	40.8 ± 0.6		
		537.45	30.5 ± 0.4		
		803.10	99.0 ± 1.4		
		881.01	66.2 ± 1.0		
		895.12	15.67 ± 0.22		
		1098.26	13.51 ± 0.20		
^{205}Bi	15.31 ± 0.04 d	703.45	31.1 ± 0.4	^{209}Bi(p, $p4n$)^{205}Bi	−29.48
		987.66	16.1 ± 0.3		
		1764.30	32.5 ± 0.7		
^{204}Bi	11.22 ± 0.1 h	374.76	82 ± 8	^{209}Bi(p, $p5n$)^{204}Bi	−37.97
		899.15	99 ± 12		
		983.98	59 ± 6		
^{203}Bi	11.76 ± 0.05 h	820.2	30.0 ± 2.5	^{209}Bi(p, $p6n$) ^{203}Bi	− 45.16
		825.2	14.8 ± 1.2		
		847.2	8.6 ± 0.7		
		896.9	13.2 ± 1.1		

TABLE III. Measured yields of monitor reactions together with measured proton beam intensities.

Experiment	Method	Reaction	Irradiation time (s)	Production yield (Bq)	Beam intensity (protons/s)
First	Activation analysis	^{27}Al(p, 3pn)^{24}Na	240	8526.2 ± 107.5	(3.66 ± 0.26)×10^{11}
Second		^{27}Al(p, 3pn)^{24}Na	25	1385.8 ± 775.6	(6.14 ± 0.61)×10^{11}
		^{197}Au(p, pn)^{196}Au		476.6 ± 9.5	(5.89 ± 0.59)×10^{11}
		^{197}Au(p, $p3n$)^{194}Au		1805.3 ± 43.6	(6.00 ± 0.60)×10^{11}

TABLE IV. Different nuclear level density models implemented in the TALYS code.

Phenomenological	Microscopic
Default: Constant temperature model (CTM) [21]+Fermi gas model (FGM) [22]	LDM-4: Microscopic level densities on the basis of Hatree-Fock calculations [31]
LDM-2: Back-shifted Fermi gas model (BFM) [22]	LDM-5: Hilaire and Goriely microscopic combinatorial Model [32]
LDM-3: Generalized superfluid model (GSM) [33]	LDM-6: Microscopic level densities based on temperature-dependent Hartree-Fock-Bogoliubov [34]

TABLE V. Measured cross sections of Po radionuclei produced from the ^{209}Bi(p, xn) reactions. "*Ind*" stands for independent cross section.

	$\sigma \pm \Delta\sigma$ (mb)			
$E \pm \Delta E$ (MeV)	^{207}Po^{Ind}	^{206}Po^{Ind}	^{205}Po^{Ind}	^{204}Po^{Ind}
43.1 ± 1.6	249.4 ± 26.5	1088.6 ± 110.0	52.3 ± 6.8	
44.1 ± 1.6	177.2 ± 17.9	1100.4 ± 113.3	112.4 ± 15.6	21.0 ± 2.1
47.5 ± 1.4	180.8 ± 19.1	788.8 ± 80.6	435.6 ± 49.7	
50.8 ± 1.5	141.9 ± 14.3	331.6 ± 63.8	875.8 ± 105.5	
54.7 ± 1.1	90.0 ± 9.6	248.4 ± 24.9	683.3 ± 81.3	104.2 ± 9.8
57.0 ± 1.1	115.8 ± 11.8	233.1 ± 23.8	593.4 ± 72.2	
61.3 ± 0.8	79.4 ± 8.3	171.5 ± 17.4	267.1 ± 29.7	380.2 ± 45.0
62.8 ± 0.8	83.5 ± 8.4	159.4 ± 16.2	238.2 ± 29.2	
67.4 ± 0.3	67.3 ± 7.8	139.0 ± 14.1	151.2 ± 16.9	307.3 ± 35.4
68.1 ± 0.3		135.3 ± 13.8		

III. RESULTS AND DISCUSSION

The measured independent and cumulative cross sections values and their uncertainties are listed in Tables V and VI. The excitation functions of investigated radionuclei are illustrated in Figs. 1–9, including our previous work [13] and other existing measured data together with nuclear model calculations. A deviation between our previous and present measured cross-section data was observed at the energy range of 67 to 72 MeV. The possible reason of the deviation could come from the contribution of low-energy protons to the reaction cross sections in our previous work. These low-energy protons have an energy of 72.0 ± 2.0 MeV that impinge on to the fourth Bi activation foil, while, for the new measurement, incident protons impinge on the first activation Bi foil are almost monoenergy, 67.4 ± 0.3 MeV. Activity measurement and uncertainty in the Bi activation foil thickness could result in the deviation as well.

Uncertainties of the presented cross sections were estimated as the sum in quadrature of possible individual relative uncertainties including proton beam intensity (10.2%), nuclear data (0.03–9.8%), detection efficiency (≈1%), net peak area uncertainty (<2.5%), and sample mass (0.01%). Overall uncertainties were ≈10.5% for Po radionuclei and ≈15% for Bi radionuclei. Uncertainties of measured independent cross sections of Bi radionuclei do not include the uncertainties from the decay process of Po.

A. ^{209}Bi(p, 3n)^{207}Po reaction

^{207}Po ($T_{1/2}$ = 5.80 h) decays to ^{207}Bi and ^{203}Pb via electron capture (EC, 99.98%) and α emission (0.02%), respectively. The 405.8-, 742.6-, and 992.3-keV γ rays were used to determine the ^{207}Po yields. The measured activity included the contribution of the decay of the simultaneously produced short-lived isomeric state ($T_{1/2}$ = 2.79 s; isomeric transition (IT): 100%) of ^{207}Po. Figure 1 depicts the measured cross sections for the reaction ^{209}Bi(p, 3n)^{207}Po compared to other experimental data as well as nuclear model calculations. In addition, the measured data in our interested energy range were reported by Chung *et al.* [4] and Miyano *et al.* [9]. Present data are higher than that of Miyano *et al.* [9], while they are consistent with the result reported by Chung *et al.* [4]. The present results are following a trend similar to that of our previous results. Obviously, LDM-5 and LDM-6 are in agreement with our data. However, the theoretical calculations overestimate the measured data by Miyano *et al.* [9] around the peak area. The TALYS default calculations and GSM model (LDM-3) reproduce the measured data by Miyano *et al.*

TABLE VI. Measured cross sections of Bi radionuclei produced from the ^{209}Bi(p, p xn) reactions. "*Ind*" and "*Cum*" stand for independent and cumulative cross section, respectively.

	$\sigma \pm \Delta\sigma$ (mb)							
$E \pm \Delta E$ (MeV)	^{207}Bi^{Ind}	^{207}Bi^{Cum}	^{206}Bi^{Ind}	^{206}Bi^{Cum}	^{205}Bi^{Cum}	^{204}Bi^{Ind}	^{204}Bi^{Cum}	^{203}Bi^{Cum}
43.1 ± 1.6	181.8 ± 18.9	431.0 ± 45.0						
44.1 ± 1.6			55.4 ± 11.0		192.0 ± 20.0			
47.5 ± 1.4	183.2 ± 19.3	364.0 ± 38.0	84.6 ± 19.0	163.0 ± 17.0	497.0 ± 50.6			
50.8 ± 1.5			121.0 ± 17.5	155.0 ± 15.8	965.4 ± 97.6	5.0 ± 0.5	35.0 ± 5.0	
54.7 ± 1.1	229.1 ± 24.3	319.0 ± 33.0	134.0 ± 19.0	180.0 ± 18.0	910.0 ± 92.2	12.8 ± 1.8		
57.0 ± 1.1			148.0 ± 17.3	167.0 ± 17.0	733.8 ± 77.0			
61.3 ± 0.8	234.4 ± 24.8	313.7 ± 33	143.4 ± 17.3	157.0 ± 16.0	472.0 ± 48.5	46.1 ± 6.5		
62.8 ± 0.8			138.0 ± 16.2	149.0 ± 15.0	393.4 ± 40.0			65.0 ± 8.7
67.4 ± 0.3	171.7 ± 19.0	239.0 ± 26.0	133.2 ± 15.2	149.0 ± 15.0	328.0 ± 33.2	73.5 ± 10.3	246.6 ± 34.7	311.5 ± 40.7
68.1 ± 0.3			136.0 ± 16.6	159.0 ± 16.0				356.0 ± 46.6

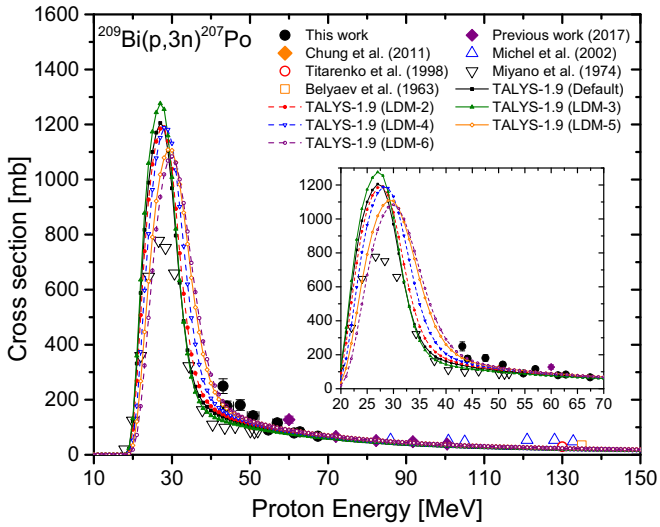

FIG. 1. Measured independent cross sections for the ^{209}Bi(p, $3n$)^{207}Po reaction compared with the previously published data together with theoretical calculations based on TALYS code. The experimental data are from Refs. [3–5,9,12,13].

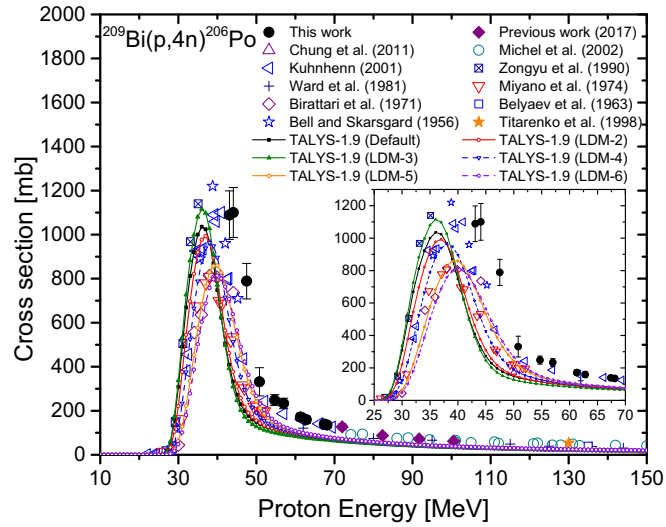

FIG. 2. Measured independent cross sections for the ^{209}Bi(p, $4n$)^{206}Po reaction compared with the previously published data together with theoretical calculations based on TALYS code. The experimental data are from Refs. [3–13].

[9] above 35 MeV. All models show an agreement to the measured data from 50 to 135 MeV.

B. ^{209}Bi(p, $4n$)^{206}Po reaction

^{206}Po ($T_{1/2}$ = 8.8 d; EC, 94.55%; and α, 5.45%) activities were measured after few days of cooling time using 286.4-, 522.5-, 807.4-, and 980.2-keV γ rays. Because of the suitable half-life of this radionuclide, its production cross sections have been measured by several researchers, including Chung *et al.* [4], Michel *et al.* [5], Kuhnhenn [8], Titarenko *et al.* [3], Zongyu *et al.* [7], Ward *et al.* [10], Miyano *et al.* [9], Birattari *et al.* [11], Belyaev *et al.* [12], and Bell and Sharsgard [6]. Figure 2 shows that our measured independent cross sections are in good agreement with the data from Ref. [8] from 55 to 70 MeV. In the peak region, our data show cross-section magnitude similar to those of Ref. [8]. Present work seems to continue a comparable tendency of the previous results. Results from Miyano *et al.* [9] and Birattari *et al.* [11] show lower cross-section values at the peak region. Nuclear model calculations underestimate our measured data. Different nuclear level density models indicate different peaks as well. LDM-3 shows comparable results to the measured values by Zongyu *et al.* [7]. On the other hand, LDM-4 is in agreement with the results measured by Kuhnhenn [8] and Bell and Skarsgard [6] up to around 35 MeV. LDM-4, LDM-5, and LDM-6 reproduce the experimental data measured by Miyano *et al.* [9] and Kuhnhenn [8] above 42 MeV. All the NLDs predict the threshold energy well.

C. ^{209}Bi(p, $5n$)^{205}Po reaction

^{205}Po ($T_{1/2}$ = 1.74 h; EC, 99.96%; and α, 0.04%) can be produced through ^{209}Bi(p, $5n$) reaction. The independent cross section of this radionuclide was obtained. ^{205}Po was identified by 836.8-, 849.8-, and 872.4-keV γ rays. Figure 3 illustrates the present results, our previous results [13], and literature data [3,4,6,12] as well as the nuclear models predictions for the ^{209}Bi(p, $5n$)^{205}Po nuclear reaction. First, data in our previous work [13] and current results are on a similar trend except for one data point at 72 MeV which is quite high. Second, our results are in reasonable agreement with the data reported by Chung *et al.* [4] and Bell and Sharsgard [6] by considering the uncertainties. Different NLD models show different peaks and TALYS-1.9 (Default) stays in between. LDM-3 predicts the maximum cross section of 890 mb at 45 MeV, while the maximum measured cross section is 875.8 at 50.8 ± 1.5 MeV. All the NLD models

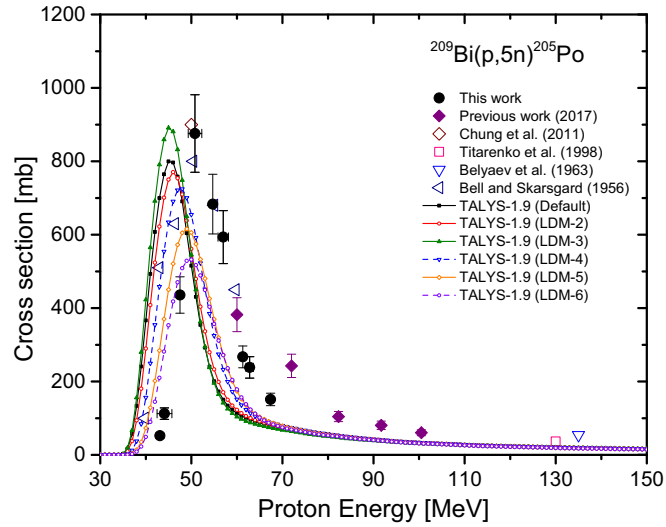

FIG. 3. Measured independent cross sections for the ^{209}Bi(p, $5n$)^{205}Po reaction compared with the previously published data together with theoretical calculations based on TALYS code. The experimental data are from Refs. [3,4,6,12,13].

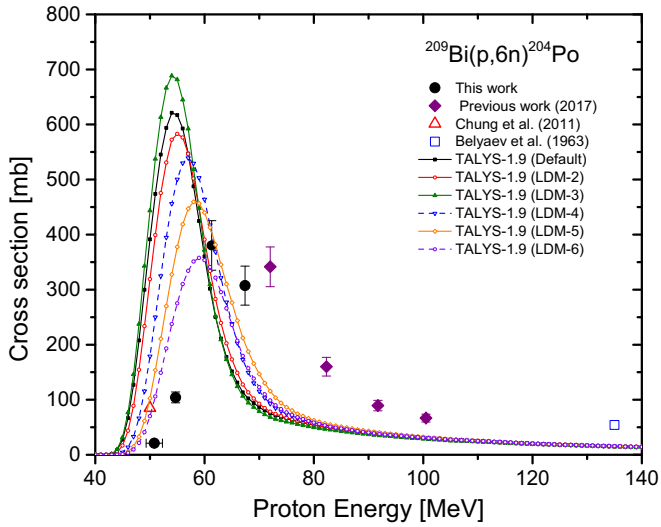

FIG. 4. Measured independent cross sections for the ^{209}Bi(p, $5n$)^{204}Po reaction compared with the previously published data together with theoretical calculations based on TALYS code. The experimental data are from Refs. [4,12,13].

show a different threshold energy than our measurement. The smallest cross-section peak is estimated by LDM-6. It seems that by applying GSM nuclear level density formalism, the theoretical calculations exhibit higher cross-section values. Phenomenological level density models are predicting the higher excitation functions than the microscopic models for this reaction.

D. ^{209}Bi(p, $6n$)^{204}Po reaction

The radionuclide ^{204}Po ($T_{1/2} = 3.519$ h; EC, 99.33%; and α, 0.67%) activities were also measured by the γ rays of 762.5 and 883.9 keV. The experimental data in the literature was rare; one data point was reported in Ref. [4] and one data point was reported in Ref. [12]. Therefore, the results in this work are new cross-section values (Fig. 4). Our earlier data seem to stay on a similar trend except for the point at 72 MeV. Cross-section estimation using nuclear models varies from around 200 mb to around 700 mb at the peak. LDM-6 show closer cross-section data to our measurement. However, all NLD models calculations underestimate the measured data at proton energies higher than 70 MeV. It was revealed that nuclear model calculations indicate different results when more particles are emitted, as can be seen from Fig. 4. For this reaction, phenomenological NLD models estimate higher cross sections than the microscopic models. More experiments are needed for this reaction to complete the excitation functions.

E. ^{209}Bi(p, $p2n$)^{207}Bi reaction

^{207}Bi ($T_{1/2} = 31.55$ yr; EC, 100%) was measured by 569.7-keV γ ray. This radionuclide could be also generated from the decay of ^{207}Po ($T_{1/2} = 5.80$ h). ^{207}Bi has a long half-life so that ^{207}Po could decay to ^{207}Bi completely. Therefore, production cross sections of ^{207}Po were subtracted from

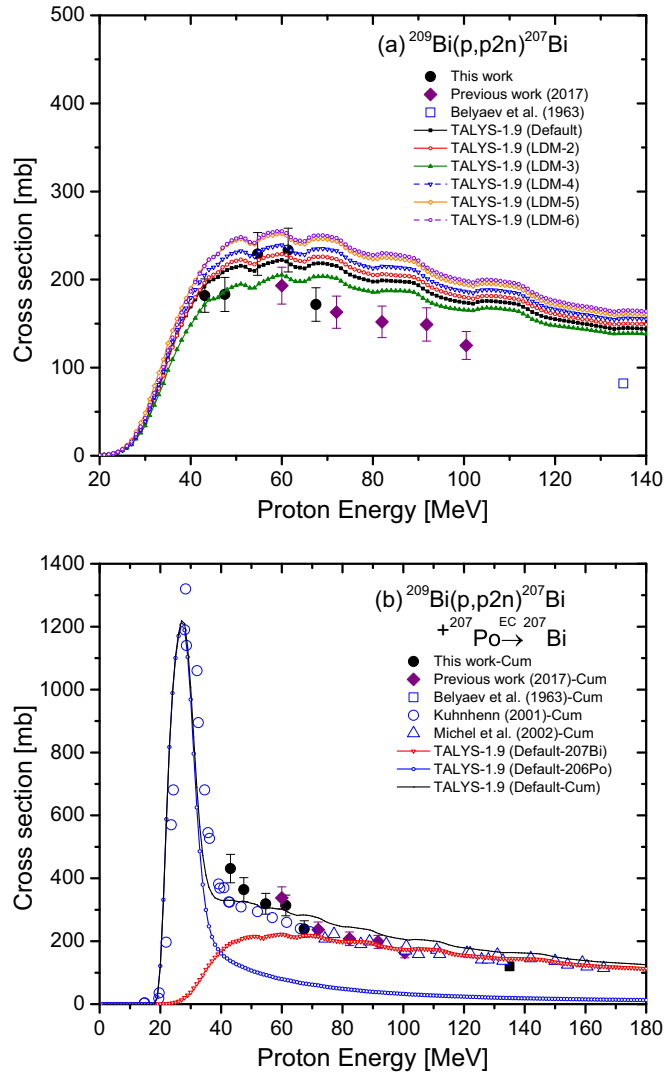

FIG. 5. (a) Measured independent cross sections and (b) measured cumulative cross sections (indicated by "Cum") for the ^{209}Bi(p, $p2n$)^{207}Bi reaction compared with the previously published data together with theoretical calculations based on TALYS code. The experimental data are from Refs. [12,13].

that of ^{207}Bi to obtain the independent cross section. Our newly measured data are consistent with our previous published data and are compared with available experimental data reported only by Belyaev *et al.* [12] [Fig. 5(a)]. Nuclear model calculations show upper values when LDM-5 or LDM-6 are used and show lower values when the LDM-3 is used. For this reaction, microscopic NLDs indicate higher cross-section values than the phenomenological models. Generally, the TALYS calculations predict the reaction threshold reasonably. However, theoretical calculations overestimate the measured cross sections above 60 MeV.

In order to compare our present data with other cumulative experimental data, the cumulative cross sections of ^{207}Bi, which can be contributed by ^{209}Bi(p, $p2n$)^{207}Bi reaction as well as the decay of ^{207}Po, are also shown in Fig. 5(b). Regarding the figure, there is good consistency between present

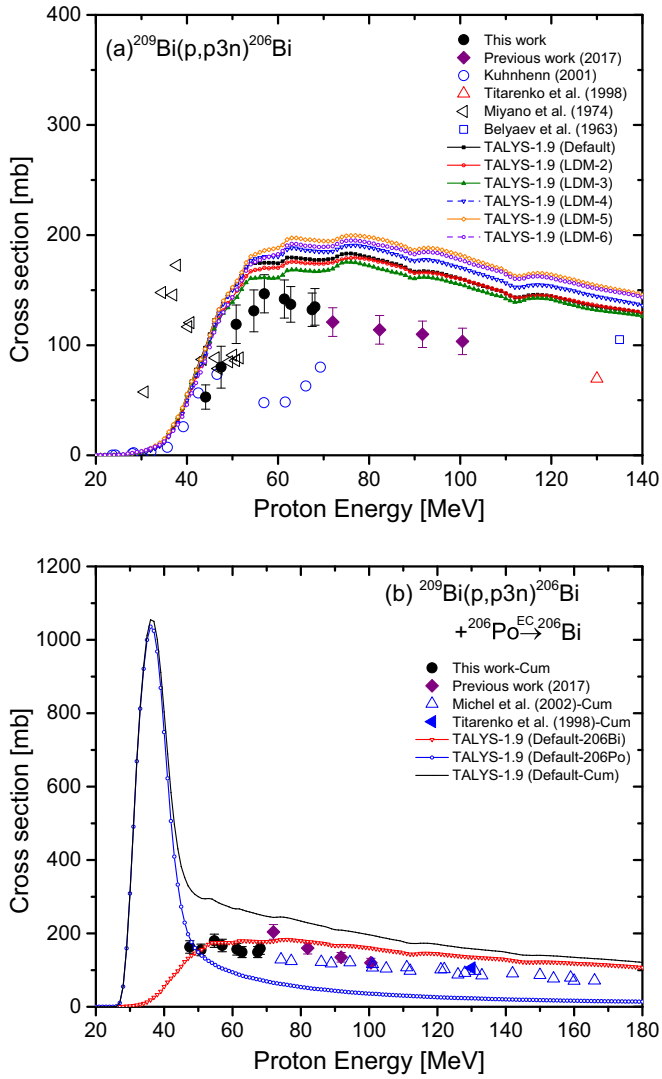

FIG. 6. (a) Measured independent cross sections and (b) measured cumulative cross sections (indicated by "Cum") for the ^{209}Bi(p, $p3n$)^{206}Bi reaction compared with the previously published data together with theoretical calculations based on TALYS code. The experimental data are from Refs. [3,5,8,9,12,13].

data and our previous data as well as the results reported by Kuhnhenn [8] and Michel *et al.* [5]. On the other hand, ^{207}Bi and ^{207}Po excitation functions from theoretical calculations in the defaults mode were summed up to obtain the cumulative reaction cross-section values [Fig. 5(b)]. TALYS calculations reveal an agreement with the measured data over the whole energy range.

F. ^{209}Bi(p, $p3n$)^{206}Bi reaction

The yield of ^{206}Bi was measured by 803.1- and 881.01-keV γ rays. ^{206}Bi has a short-lived isomeric state ($T_{1/2} = 0.89$ ms) that decays to the ground state ($T_{1/2} = 6.243$ d). ^{206}Bi production could be contributed by the decay of ^{206}Po. Present results and our earlier data are in good agreement in shape and magnitude. Additionally, determined cross sections are consistent with data by Miyano *et al.* [9] at 50 MeV [Fig. 6(a)]. However, the data around threshold are in good agreement with the results reported by Kuhnhenn [8]. In the case of nuclear model calculations using different models, they illustrate similar threshold values to the experimental data. On the other hand, for higher energies, theoretical calculations by the TALYS code overestimate the experimental data. For this reaction, microscopic level density models LDM-4, LDM-5, and LDM-6 show higher cross sections than the phenomenological models TALYS-1.9 (Default), LDM-2, and LDM-3. The cumulative cross sections are also shown and are compared to our earlier data together with the other experimental data reported by Michel *et al.* and Titarnenko *et al.* [3,5]. All experimental data seem to be on a similar trend. It is seen that after 50 MeV, the ^{206}Po cross section less contribute to the cumulative cross section as shown in Fig. 6(b). The TALYS results for ^{206}Po and ^{206}Bi were added up and are shown in comparison with the measured data. Apparently, TALYS-1.9 (Default-Cum) overestimate all experimental data slightly. There were no measured reaction cross sections around the peak ($E = 35$ MeV) for this reaction to confirm the nuclear model calculations estimation and to complete the excitation functions.

G. ^{209}Bi(p, $p4n$)^{205}Bi reaction

^{205}Bi with half-life of 15.31 d is produced from ^{209}Bi(p, $p4n$) reaction as well as the decay of ^{205}Po ($T_{1/2} = 1.74$ h). Measurement was performed with long cooling time after the irradiation so that ^{205}Po could decay to ^{205}Bi completely. Therefore, the measured cross sections were cumulative as shown in Fig. 7. The 703.45-keV γ ray was used for the measurement. Present data agree well with our previous data and also with other measured data by Refs. [3,5,8]. In order to show cumulative cross sections calculated by the TALYS code, the production cross sections of ^{205}Bi and ^{205}Po were added up and are indicated in Fig. 7. It can be seen that TALYS

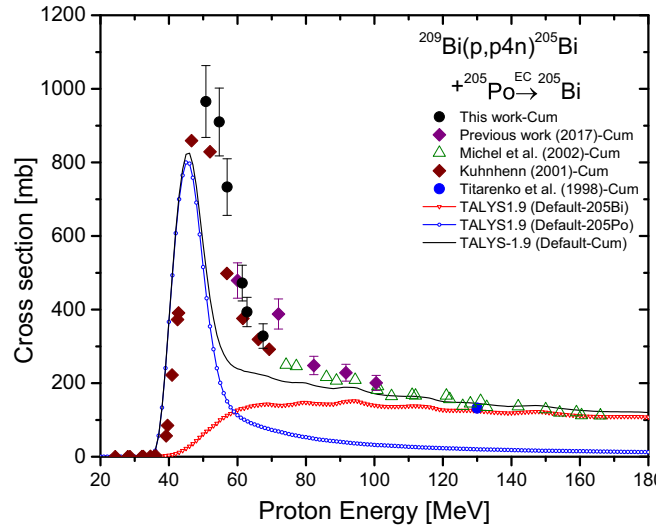

FIG. 7. Measured cumulative cross sections for the ^{209}Bi(p, $p4n$)^{205}Bi reaction compared with the previously published data together with theoretical calculations based on TALYS code. The experimental data are from Refs. [3,5,8,13].

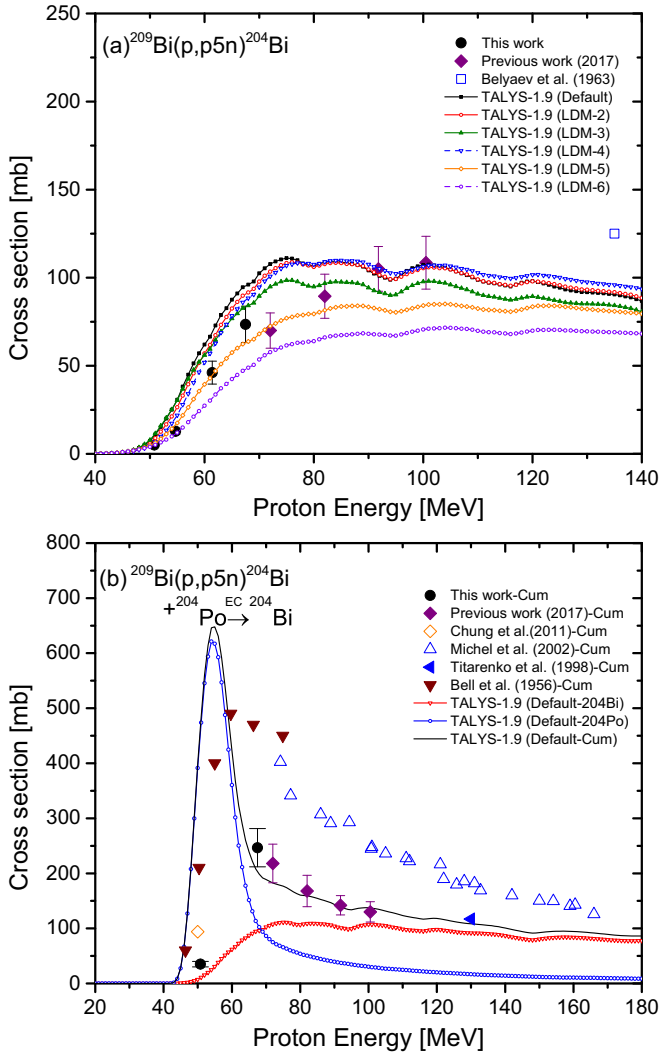

FIG. 8. (a) Measured independent cross sections and (b) measured cumulative cross sections (indicated by "Cum") for the ^{209}Bi(p, $p5n$)^{204}Bi reaction compared with the previously published data together with theoretical calculations based on TALYS codes. The experimental data are from Refs. [3–5,12,13].

predicts the reaction cross section at the threshold well. However, there is a discrepancy between theoretical calculations and experimental data between 52 and 80 MeV. At higher energies, TALYS reproduces the experimental data well. The shape of the excitation function is confirmed by our measured cross sections and the data measured by Kuhnhenn [8].

H. ^{209}Bi(p, $p5n$)^{204}Bi reaction

^{204}Bi has a ground state with half-life of 11.22 h and two short-lived metastable state with half-lives of 13 and 1.07 ms which decay to the ground state with branching ratios of 100%. ^{204}Bi could be produced from ^{209}Bi(p, $p5n$)^{204}Bi and also from the decay of ^{204}Po ($T_{1/2} = 3.519$ h). The production yield of ^{204}Bi was identified using 374.76-keV γ ray in the spectrum. The measured independent cross sections are shown in Fig. 8(a). The data in our previous work show a shape similar to that of the recent data. According to the measured data, the shape of the excitation functions for this reaction could be predicted. Nuclear model calculations based on the TALYS code show the reaction threshold well, comparing to the experimental data. Theoretical calculations could vary depending on the nuclear level density model as shown in Fig. 8(a). It is seen that LDM-5 reproduces the experimental data from threshold to 85 MeV well, underestimating the measured data at higher energies. The data presented in this work are newly measured independent cross sections. More experiments would confirm the excitation functions.

As mentioned above, ^{204}Bi could be produced from ^{209}Bi(p, $p5n$)^{204}Bi and also from the decay of ^{204}Po. Therefore, cumulative reaction cross sections were also measured to compare with the available data in the literature [Fig. 8(b)]. The present data follow the trend of our previous results [13]. However, they are far lower than the data published by Belyaev *et al.* [12] and Michel *et al.* [5]. On the other hand, calculated cumulative cross sections performed by TALYS code show a good agreement with data reported by us in this work and our preceding work [13] as well as with the single data point at 130 MeV measured by Titarenko *et al.* [3].

I. ^{209}Bi(p, $p6n$)^{203}Bi reaction

^{203}Bi ($T_{1/2} = 11.76$ h; EC, 100%) was measured using 820.2-keV γ rays after a few hours of cooling time. This radionuclide could be generated through ^{209}Bi(p, $p6n$) reaction and also from the decay of ^{203}Po ($T_{1/2} = 36.7$ m). Cumulative cross sections could be measured and are shown in Fig. 9 together with the previously published data. The present data underestimate the results measured by Bell *et al.* [6]. For the energies lower than 70 MeV, the contribution cross section of ^{203}Po to the total production cross section become more dominant and reaches a maximum value of 425 mb based on TALYS calculations. TALYS results in the default

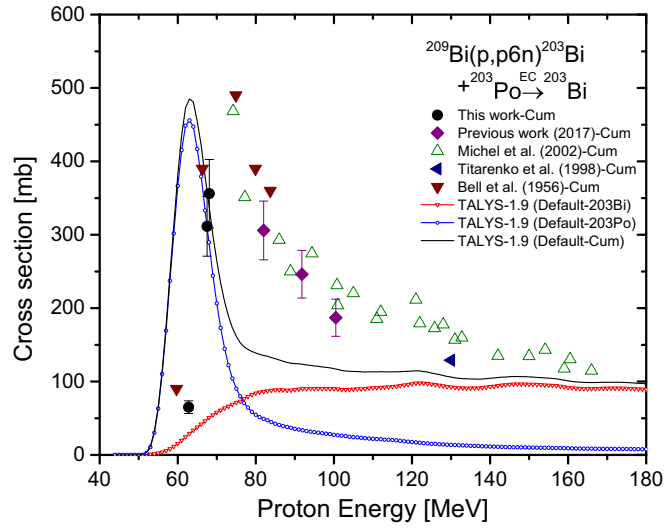

FIG. 9. Measured cumulative cross sections (indicated by "Cum") for the ^{209}Bi(p, $p6n$)^{203}Bi reaction compared with the previously published data together with theoretical calculations based on TALYS code. The experimental data are from Refs. [3,5,6,13].

mode were summed up for production of ^{203}Bi and ^{203}Po to be compared with measured cumulative cross sections. Theoretical calculations by TALYS predict the peak at lower energies than the experimental data. For the higher energies, nuclear model calculations underestimate the experimental data. It is seen that there is a lack of data around the peak and threshold for this reaction. More measurements at these areas could improve the excitation functions.

IV. CONCLUSIONS

Cross sections of the nuclear reactions ^{209}Bi(p, xn)^{207,206,205,204}Po and ^{209}Bi(p, pxn)^{207,206,205,204,203}Bi were measured between 40 and 69 MeV. More than 50 cross-section data points were measured. We have extended the excitation functions of the mentioned reactions over the energy range of 40 to 100 MeV. Our measured data in this work were consistent with our previous work and other experimental results in the literature.

In addition, nuclear model calculations were performed using the TALYS code, applying six different nuclear level density models. The measured independent and cumulative cross sections were compared to the theoretical calculations. For the ^{209}Bi(p, xn) reactions, when the number of outgoing neutrons increases, the deviation between theoretical calculations and measurements increases correspondingly. Moreover, phenomenological level density models estimated higher cross-section values than the microscopic models. On the other hand, for ^{209}Bi(p, pxn) reactions, TALYS calculations showed reasonable agreement to the measured data and, in general, microscopic level density models predicted higher cross sections than the phenomenological models.

For the ^{209}Bi(p, $3n$)^{207}Po reaction, LDM-5 and LDM-6, which are microscopic NLDs, were in agreement with our measured data. In the case of ^{209}Bi(p, $4n$)^{206}Po and ^{209}Bi(p, $5n$)^{205}Po reactions, LDM-3 showed the cross-section magnitude similar to the experimental data. However, the peak energy was slightly different. LDM-3 was closer to the measured cross section for ^{209}Bi(p, $p2n$)^{207}Bi reaction. All the NLD models could predict the threshold energy for the ^{209}Bi(p, $p3n$)^{206}Bi and ^{209}Bi(p, $p5n$)^{204}Bi reactions quite well. In case of the ^{209}Bi(p, $p5n$)^{204}Bi reaction, LDM-5 was in agreement with the measurement up to 85 MeV. The cumulative production cross sections of ^{207}Bi were reproduced well by the TALYS default calculations.

It could be concluded that NLDs were effective parameters in the cross-section estimation. It implies that nuclear level density tables used in TALYS code need to be improved as they could affect the reaction cross section significantly in this study. The measured excitation function can boost the nuclear reaction models. These obtained data can also improve nuclear data libraries for bismuth.

ACKNOWLEDGMENTS

The authors would like to thank the KOMAC team for their cooperation during the experiment. We also thank our colleague Dr. Y. U. Kye for his help during the experiment. This work is supported by the Nuclear Safety Research Program through the Korea Foundation Of Nuclear Safety (KOFONS), granted financial resources from the Nuclear Safety and Security Commission (NSSC) of Republic of Korea (Grants No. 1303026 and No. 1603005).

[1] M. Gloris, R. Michel, U. Herpers, F. Sudbrock, and D. Filges, Nucl. Instrum. Methods Phys. Res. B **113**, 429 (1996).
[2] N. Singh, K. J. Singh, K. Singh, and H. Singh, Nucl. Instrum. Methods Phys. Res. B **225**, 305 (2004).
[3] Y. Titarenko, O. Shvedov, M. Igumnov, S. Mashnik, E. Karpikhin, V. Kazaritsky, V. Batyaev, A. Koldobsky, V. Zhivun, A. Sosnin, R. Prael, M. Chadwick, T. Gabriel, and M. Blann, Nucl. Instrum. Meth. Phys. Res. A **414**, 73 (1998).
[4] Y. Chung, C. Lee, K. Nahm, K. Joo, J. Chai, and K. Chun, J. Kor. Phys. Soc. **59**, 1007 (2011).
[5] R. Michel, M. Gloris, J. Protoschill, U. Herpers, J. Kuhnhenn, F. Sudbrock, P. Malmborg, and P. Kubik, J. Nucl. Sci. Techno. L **39**, 242 (2002).
[6] R. Bell and H. Skarsgard, Can. J. Phys. **34**, 745 (1956).
[7] B. Zongyu, C. J. Inhua, M. Jiangchen, and H. Shengnian, Chin. J. Nucl. Phys. **12**, 55 (1990).
[8] J. Kuhnhenn, Thin target cross sections for proton-induced production of radionuclides from lead and bismuth over the proton energy range from 9 to 71 MeV, Ph.D. thesis, University of Koeln, Germany, 2001.
[9] K. Miyano, M. Sekikawa, T. Kaneko, and M. Nomoto, Nucl. Phys. A **230**, 98 (1974).
[10] T. E. Ward, P. P. Singh, D. L. Friesel, A. Yavin, A. Doron, J. M. D'Auria, G. Sheffer, and M. Dillig, Phys. Rev. C **24**, 588 (1981).
[11] C. Birattari, E. Gadioli, A. Strini, G. Strini, G. Tagliaferri, and L. Zetta, Nucl. Phys. A **166**, 605 (1971).
[12] B. I. Belyaev, A. V. Kalyamin, and A. N. Murin, Bull. Russ. Acad. Sci. Phys. **27**, 907 (1963).
[13] L. Mokhtari Oranj, N. S. Jung, M. Bakhtiari, A. Lee, and H. S. Lee, Phys. Rev. C **95**, 044609 (2017).
[14] A. Koning, S. Hilaire, and M. Duijvestijn, in *Proceedings of the International Conference on Nuclear Data for Science and Technology*, edited by O. Bersillon, F. Gunsing, E. Bauge, R. Jacqmin, and S. Leray (EPD Science, Nice, France, 2007), pp. 211–214 [http://www.talys.eu/download-talys].
[15] J. F. Ziegler, M. Ziegler, and J. Biersack, Nucl. Instrum. Methods Phys. Res. B **268**, 1818 (2010).
[16] GENIE 2000 basic spectroscopy software, version 3.2 [www.Canberra.com].
[17] A. Ferrari, P. R. Sala, A. Fasso, and J. Ranft, in *CERN-2005-10 (2005), INFN/TC_05/11, SLAC-R-773* [http://www.fluka.org/].
[18] Y. E. Titarenko, S. P. Borovlev, M. A. Butko, V. M. Zhivun, K. V. Pavlov, V. I. Rogov, A. Y. Titarenko, R. S. Tikhonov, S. N. Florya, and A. B. Koldobskiy, Phys. Atom. Nucl. **74**, 507 (2011).

[19] F. Szelecsényi, G. Steyn, Z. Kovács, and T. Van der Walt, in *International Conference on Nuclear Data for Science and Technology* (EDP Sciences, Nice, France, 2007), pp. 1259–1262.
[20] ENSDF database [http://www.nndc.bnl.gov/ensarchivals/].
[21] A. Gilbert and A. G. W. Cameron, Can. J. Phys. **43**, 1446 (1965).
[22] W. Dilg, W. Schantl, H. Vonach, and M. Uhl, Nucl. Phys. A **217**, 269 (1973).
[23] A. Koning and J. Delaroche, Nucl. Phys. A **713**, 231 (2003).
[24] J. Kopecky and M. Uhl, Phys. Rev. C **41**, 1941 (1990).
[25] A. Spyrou, A. Lagoyannis, P. Demetriou, S. Harissopulos, and H.-W. Becker, Phys. Rev. C **77**, 065801 (2008).
[26] S. Harissopulos, A. Spyrou, V. Foteinou, M. Axiotis, G. Provatas, and P. Demetriou, Phys. Rev. C **93**, 025804 (2016).
[27] E. Bauge, J. P. Delaroche, and M. Girod, Phys. Rev. C **63**, 024607 (2001).
[28] W. Hauser and H. Feshbach, Phys. Rev. **87**, 366 (1952).
[29] M. Bakhtiari, M. Sadeghi, M. K. Bakht, and H. Ghafoori-Fard, Phys. Rev. C **87**, 034621 (2013).
[30] M. Sadeghi, M. Bakhtiari, M. K. Bakht, M. Anjomrouz, and L. Mokhtari, Phys. Rev. C **85**, 034605 (2012).
[31] S. Goriely, F. Tondeur, and J. Pearson, At. Data Nucl. Data Tables **77**, 311 (2001).
[32] S. Goriely, S. Hilaire, and A. J. Koning, Phys. Rev. C **78**, 064307 (2008).
[33] A. V. Ignatyuk, J. L. Weil, S. Raman, and S. Kahane, Phys. Rev. C **47**, 1504 (1993).
[34] S. Hilaire, M. Girod, S. Goriely, and A. J. Koning, Phys. Rev. C **86**, 064317 (2012).